Int. J. Heat Mass Transfer. Vol. 31, No. 4, pp. 723–730, 1988
Printed in Great Britain

0017–9310/88 $3.00+0.00

Correlation between the longitudinal velocity fluctuation and temperature fluctuation in the near-wall region of a turbulent boundary layer

R. A. ANTONIA and L. V. KRISHNAMOORTHY
Department of Mechanical Engineering, University of Newcastle, N.S.W., 2308, Australia

and

L. FULACHIER
Institut de Mécanique Statistique de la Turbulence, Université d'Aix-Marseille, 13003 Marseille, France

(*Received* 1 *May* 1987 *and in final form* 1 *July* 1987)

Abstract—Measurements of the longitudinal velocity fluctuation u and of the temperature fluctuation θ in a turbulent boundary layer indicate a strong correlation between u and θ in the immediate vicinity of the wall, the absolute value of the correlation coefficient approaching unity at the wall. The importance of low-speed or high-temperature streaks is examined and quantified by considering joint probability and spectral density functions of u and θ.

INTRODUCTION

THE EARLIER flow visualization of Hama [1] and the later more detailed visualization of ref. [2] highlighted the relatively strong organization of the wall-adjacent region of a turbulent boundary layer. Low-speed fluid streaks were observed to be elongated in the streamwise direction and separated in the spanwise direction by somewhat wider zones of higher-speed fluid. When the wall is slightly heated, one would expect the low-speed streaks to coincide to a good approximation, with regions of relatively warm fluid, whereas the high-speed zones would be more likely associated with relatively cool fluid arriving from regions further away from the wall. Orlando *et al.* [3] argued that since the flow-oriented streaks retained their identity for a long time, a high correlation was expected between the longitudinal velocity fluctuation u and the temperature fluctuation θ (strictly $-\theta$ since different boundary conditions apply to velocity and temperature as the zero velocity wall is heated). They suggested that $\rho_{u\theta}$, the correlation coefficient between u and $-\theta$ should approach unity at the wall but did not present experimental verification of this. The data (Fig. 1) of ref. [4] in a pipe flow and ref. [5] on a flat plate implied that relatively high values of $\rho_{u\theta}$ may be attained near $y = 0$ but these data do not extend to sufficiently small values of y^+ to allow reasonable extrapolation to the wall. A similar inference could be made from the earlier data of ref. [6]† on a flat plate. However, measurements in a pipe flow by ref. [7] and more especially ref. [8] indicate that a maximum in $\rho_{u\theta}$ is reached at $y^+ \simeq 10$ before a rapid decrease towards zero at the wall.

Bremhorst and Bullock [4] noted that at the wall the streaks can be expected to show near perfect correlation between u and $-\theta$. These authors also presented cross-spectral data, indicating a near perfect correlation coefficient between u and $-\theta$ at low wave numbers. The recent and interesting experiments of ref. [9] involving simultaneous visualizations of the instantaneous wall temperature and of the near-wall flow, indicated that low-speed streaks coincided, with high probability, with high-temperature streaks whereas high-speed streaks corresponded closely with low-temperature streaks. All of the previous evidence tends to support an expectation for a high correlation between u and $-\theta$, in the immediate vicinity of the wall, in contrast with the trend of the data of refs. [7, 8]. The present measurements were made in order to clarify the magnitude of $\rho_{u\theta}$ in the near-wall region, mainly $0 \leqslant y^+ \lesssim 40$. Joint probability density functions and cross-spectra of u and θ are presented and discussed in the context of the near-wall flow structure.

EXPERIMENTAL ARRANGEMENT

The measurements were made in a suction type wind tunnel at a nominal free stream velocity U_1 of 9 m s^{-1}. The boundary layer developed over the heated aluminium floor of the working section (width = 0.6 m, height = 0.12 m, length = 1.8 m). Details of the tunnel, heated plate and basic instrumentation are given in ref. [10]. With constant wall heat flux con-

† Johnson's data have not been included in Fig. 1 as we were not able to estimate y^+ unambiguously from the information given in that paper.

NOMENCLATURE

Co co-spectrum between u and θ

Coh spectral coherence between u and θ, $(Co^2+Q^2)/\phi_u\phi_\theta$

d_{cw} diameter of cold wire [m]

f frequency [Hz]

$F(\alpha)$ flatness factor of fluctuation $\alpha \equiv \overline{\alpha^4}/\overline{\alpha^2}^2$

p kinematic pressure fluctuation [$m^2\ s^{-2}$]

$\hat{p}(u)$, $\hat{p}(\theta)$ probability density functions of u and θ normalized so that

$$\int_{-\infty}^{\infty} \hat{p}(u)\,du = 1 \quad \text{or} \quad \int_{-\infty}^{\infty} \hat{p}(\theta)\,d\theta = 1$$

$\hat{p}(u,\theta)$ joint probability density function between u and θ, normalized so that

$$\int\int_{-\infty}^{\infty} \hat{p}(u,\theta)\,du\,d\theta = 1$$

$\hat{p}(u/\theta)$ conditional probability density function of u, for a fixed value of θ

Q quadrature spectrum between u and θ

$S(\alpha)$ skewness fluctuation $\alpha \equiv \overline{\alpha^3}/\overline{\alpha^2}^{3/2}$

T instantaneous temperature [K]

$\bar{T}$ mean temperature [K]

u,v,w velocity fluctuations in x,y,z directions, respectively [$m\ s^{-1}$]

$\overline{u\theta}$ average longitudinal heat flux (thermometric) [($m\ s^{-1}$) K]

U instantaneous velocity in x direction [$m\ s^{-1}$]

$\bar{U},\bar{V},\bar{W}$ mean velocities in x,y,z directions, respectively [$m\ s^{-1}$]

U_τ friction velocity, $\tau_w^{1/2}$ [$m\ s^{-1}$]

x streamwise direction

y direction normal to wall

z spanwise direction.

Greek symbols

$\alpha_i, \beta_i, \gamma_i, \delta_i$ dimensionless coefficients in equations (6)–(9), respectively

γ fluid thermal diffusivity [$m^2\ s^{-1}$]

δ boundary layer thickness [m]

δ_2 momentum thickness,

$$\int_0^{\infty} \bar{U}/U_1(1-\bar{U}/U_1)\,dy\ [\text{m}]$$

θ temperature fluctuation [K]

ν fluid kinematic viscosity [$m^2\ s^{-2}$]

$\rho_{u\theta}$ dimensionless correlation coefficient, $-\overline{u\theta}/\overline{u^2}^{1/2}\overline{\theta^2}^{1/2}$

τ_w kinematic wall shear stress [$m^2\ s^{-2}$]

ϕ_α spectral density of fluctuation α, normalized such that

$$\int_0^{\infty} \phi_\alpha(\omega)\,d\omega = 1$$

ω circular frequency, $2\pi f$ [s^{-1}].

Other symbol

$\overline{(\ )^2}^{1/2}$ r.m.s. value of quantity within parentheses.

Superscript

$^+$ normalization by wall variables, e.g. $y^+ \equiv yU_\tau/\nu$.

ditions, the temperature difference between the wall and the free stream ($T_w - T_1$) was approximately 9.6 K at the measuring station ($x = 1.4$ m, where x is measured from the beginning of the working section). The thermal layer thickness was equal to the boundary layer thickness δ(= 28 mm). The momentum thickness Reynolds number $U_1\delta_2/\nu$ was equal to 2000. Since the walls of the working section were parallel, the boundary layer developed with a small favourable pressure gradient, the magnitude $(\nu/U_\tau^3)\,dp/dx$ remaining constant ($\simeq -10^{-3}$) in the range $0.3 < x < 1.8$ m.

The fluctuations u and θ were measured with a pair of parallel wires, one hot and one cold, at the same nominal distance from the wall. The wires were aligned in the spanwise z direction and were therefore normal to the mean flow direction. The prongs supporting the wires were inclined at a relatively shallow angle ($< 10°$) to the wall to minimize any possibility of flow interference. Both wires were etched from Wollaston, the upstream cold wire having a diameter d_{cw} equal to 0.63 μm and an active length of 1.1 mm and the downstream hot wire having a diameter of 5 μm and an active length of 0.9 mm. The streamwise separation was about 0.4 mm or about 635 cold wire diameters.

The hot wire was operated with a DISA 55M10 constant temperature circuit with a resistance ratio of 1.6, corresponding to a wire temperature of about 375 K. The cold wire was operated with an in-house circuit, with a constant current of 0.1 mA. Suitable d.c. offset voltages and amplifications were applied to the instantaneous voltages from the two circuits. The resulting signals were low-pass filtered at a cutoff frequency of 1 kHz (per channel) and digitized at a sampling frequency of 2 kHz into a PDP 11/34 computer. The voltages from the two circuits were monitored through the experiment on an NEC computer, using a

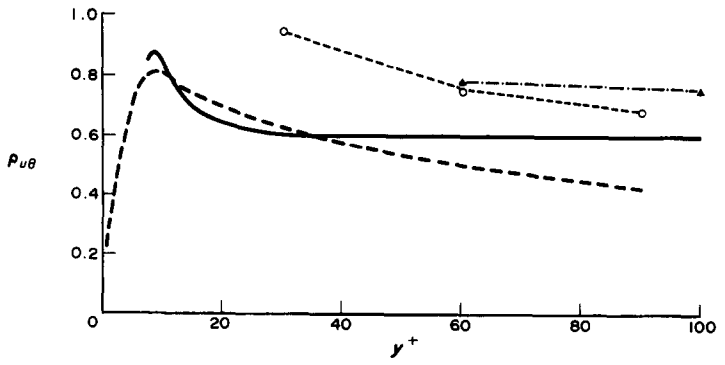

FIG. 1. Existing data for the correlation coefficient $\rho_{u\theta}$ in the region $0 < y^+ < 100$. —·—, Bremhorst and Bullock [4]; ▲, Fulachier [5]; ——, Hishida and Nagano [7]; ○, Eléna [8].

sampling frequency of 10 Hz, which was also used for calibrating the two-wire probe.

The parallelism of the wires to the wall and the distance of these wires from the polished aluminium wall were obtained using a cathetometer. This distance could be estimated within ± 0.01 mm. The probe was displaced in the y direction using a traversing mechanism fitted out with a dial gauge with a least count of 0.01 mm. The hot wire was calibrated in the free stream of the tunnel against a Pitot tube connected to a Baratron pressure transducer. The temperature coefficient of the Wollaston wire was estimated, by measurement in the core of a heated jet, to be $1.60 \times 10^{-3}\ \mathrm{K}^{-1}$.

Hishida and Nagano [11] found that the wake of the upstream wire stopped affecting the downstream hot wire when the streamwise separation exceeded 150 d_{cw} and noted that this finding was not significantly dependent on the Reynolds number based on d_{cw}. The present streamwise separation of 635 d_{cw} amply satisfies this criterion, although it should be recalled that Hishida and Nagano's [11] result does not take into account the possible effect of shear on the wake of the upstream wire. Since statistics of u obtained with the two-wire probe in the near-wall region were in close agreement with those obtained with a single hot wire, the possibility of interference due to the upstream wire or its supports in a relatively strong shear zone was ruled out. We also examined the possibility of the downstream hot wire affecting the performance of the upstream cold wire by radiation. When the hot wire was switched off the mean voltage of the cold wire changed by an amount, independent of location in the near-wall region, corresponding to a decrease in mean temperature of about 20%. However, the probability and spectral density functions of θ, normalized to unity area, were identical, irrespective of whether the hot wire was active or not, so that the statistics of the temperature fluctuation were not affected by the radiation from the hot wire. When applying the temperature correction to the hot-wire voltage, the correct mean temperature was used, rather than the mean temperature indicated by the cold wire when the hot wire was active. However, statistics of u were not sensitive to this correction. The ratio of hot-wire length to hot-wire diameter is sufficiently large (180) to avoid possible end effects. For the cold wire, the length to diameter ratio is about 1700. In ref. [12] it was found that, throughout the near-wall region and for experimental conditions similar to the present ones, the r.m.s. skewness and flatness factors of θ were essentially unchanged for cold wires with a ratio in the range 650–1700. It is possible however, that the previous result may be due to a compensation, as the wire length increases, between the attenuation of the high frequency end of the spectrum and the improved response at the low frequency end. The present cold wire has a length of 28 wall units which, although smaller than the average spanwise spacing ($\simeq 100$) of low-speed streaks, would be of the same order as the spanwise extent of these streaks. Iritani *et al.* [9] found that, at $y^+ \simeq 5.5$, the normalized correlation

$$\overline{\theta(z)\theta(z+\Delta z)}/\overline{\theta^2}^{1/2}(z)\overline{\theta^2}^{1/2}(z+\Delta z)$$

obtained with thermocouples of 50 μm diameter, first crossed zero at $\Delta z^+ \simeq 30$. A systematic investigation of the effect of cold wire length on quantities such as $\overline{\theta^2}^{1/2}$, $\overline{\theta(z)\theta(z+\Delta z)}$, $\overline{u\theta}$ would clearly be desirable.

CORRELATION COEFFICIENT BETWEEN u AND θ

Some insight into the behaviour of $\overline{u\theta}$ in the immediate vicinity of the wall can be inferred from a Taylor series expansion of the product $u\theta$ away from the wall. We can start with expansions for u and θ and then form their product (terms higher than y^3 are not shown in all the expansions given below)

$$u = \left(\frac{\partial u}{\partial y}\right)y + \left(\frac{\partial^2 u}{\partial y^2}\right)\frac{y^2}{2} + \left(\frac{\partial^3 u}{\partial y^3}\right)\frac{y^3}{6} \qquad (1)$$

$$\theta = \left(\frac{\partial \theta}{\partial y}\right)y + \left(\frac{\partial^2 \theta}{\partial y^2}\right)\frac{y^2}{2} + \left(\frac{\partial^3 \theta}{\partial y^3}\right)\frac{y^3}{6} \qquad (2)$$

where the coefficients in parentheses are evaluated at $y = 0$. In general, these coefficients depend on x, z

and t, although their average value should be zero (e.g. refs. [13, 14]). Use can be made of the transport equations for the longitudinal velocity fluctuation and the temperature fluctuation equation to evaluate the coefficients of y^2. At $y = 0$, the equation for u reduces to (e.g. p. 220 of ref. [15])

$$\frac{\partial p}{\partial x} = \nu \frac{\partial^2 u}{\partial y^2}. \tag{3}$$

The transport equation for θ written out in full below for a two-dimensional mean flow [i.e. $\bar{W} = 0$, $\partial(\overline{\ })/\partial z = 0$]

$$\frac{\partial \theta}{\partial t} + \bar{U}\frac{\partial \theta}{\partial x} + \bar{V}\frac{\partial \theta}{\partial y} + u\frac{\partial \bar{T}}{\partial x} + v\frac{\partial \bar{T}}{\partial y} + u\frac{\partial \theta}{\partial x} + v\frac{\partial \theta}{\partial y} + w\frac{\partial \theta}{\partial z} = \gamma\left(\frac{\partial^2 \theta}{\partial x^2} + \frac{\partial^2 \theta}{\partial y^2} + \frac{\partial^2 \theta}{\partial z^2}\right) + \frac{\partial}{\partial x}\overline{u\theta} + \frac{\partial}{\partial y}\overline{v\theta}$$

reduces to

$$\frac{\partial^2 \theta}{\partial y^2} = 0 \tag{4}$$

at $y = 0$. Multiplying equation (1) with equation (2) and taking into account boundary conditions (3) and (4) yields, to order y^4

$$u\theta = \left(\frac{\partial u}{\partial y}\right)\left(\frac{\partial \theta}{\partial y}\right)y^2 + \left(\frac{\partial \theta}{\partial y}\right)\left(\frac{\partial p}{\partial x}\right)\frac{y^3}{2\nu}. \tag{5}$$

After averaging and normalizing, we obtain

$$\overline{u^+\theta^+} = \alpha_1 y^{+2} + \alpha_2 y^{+3} \tag{6}$$

where

$$\alpha_1 = \overline{(\partial u^+/\partial y^+)(\partial \theta^+/\partial y^+)}$$

and

$$\alpha_2 = \tfrac{1}{2}\overline{(\partial \theta^+/\partial y^+)(\partial p^+/\partial x^+)}.$$

Squaring and averaging equations (1) and (2) yields, after taking the square root

$$\overline{u^{+2}}^{1/2} = \beta_1 y^+ + \beta_2 y^{+2} + \beta_3 y^{+3} \tag{7}$$

where

$$\beta_1 = \overline{(\partial u^+/\partial y^+)^2}^{1/2},$$

$$\beta_2 = \overline{(\partial u^+/\partial y^+)(\partial p^+/\partial x^+)}/2\beta_1,$$

$$\beta_3 = \overline{(\partial u^+/\partial y^+)(\partial^3 u^+/\partial y^{+3})}/6\beta_1 + \overline{(\partial p^+/\partial x^+)^2}/8\beta_1$$

$$\overline{\theta^{+2}}^{1/2} = \gamma_1 y^+ + \gamma_2 y^{+3} \tag{8}$$

where

$$\gamma_1 = \overline{(\partial \theta^+/\partial y^+)^2}^{1/2}$$

and

$$\gamma_2 = \overline{(\partial \theta^+/\partial y^+)(\partial^3 \theta^+/\partial y^{+3})}/6\gamma_1.$$

The absence of a quadratic term in equation (8) reflects the condition expressed by relation (4). The correlation coefficient $\rho_{u\theta}$ can then be obtained from equations (6)–(8), and written in the following form:

$$\rho_{u\theta} = \delta_1 + \delta_2 y^+ + \delta_3 y^{+2} + \delta_4 y^{+3} \tag{9}$$

where δ_1 is given by

$$\delta_1 = -\frac{\alpha_1}{\beta_1\gamma_1} = -\frac{\overline{\left(\frac{\partial u^+}{\partial y^+}\right)\left(\frac{\partial \theta^+}{\partial y^+}\right)}}{\overline{\left(\frac{\partial u^+}{\partial y^+}\right)^2}^{1/2}\,\overline{\left(\frac{\partial \theta^+}{\partial y}\right)^2}^{1/2}} \tag{10}$$

and represents the correlation coefficient between the wall fluctuating velocity gradient and the wall fluctuating temperature gradient.

Measured distributions of $-\overline{u^+\theta^+}$ and $-\rho_{u\theta}$ are shown in Fig. 2. The main features of these distributions are the large peak magnitude of $-\overline{u^+\theta^+}$ and the approach to unity of $-\rho_{u\theta}$ at the wall. As in ref. [7], $-\overline{u^+\theta^+}$ is maximum in the buffer layer, near $y^+ \simeq 15$, and decreases rapidly towards the wall. The present maximum is however almost twice as large as that reported by ref. [7]. The coefficient $-\rho_{u\theta}$ increases throughout the buffer layer and viscous sublayer towards a value which is very close to unity at $y^+ = 0$. This behaviour differs substantially from the data of ref. [8] but supports an extrapolation to the wall of the trend suggested by the data of refs. [4, 5].

Estimates of the coefficients in equations (6)–(9) were obtained from least-square regressions to measurements close to the wall. Results are given in Table 1 for the coefficients of the first terms in equations (6)–(9) and for three values of the upper limit of the y^+ range. Although β_1 is slightly more affected than α_1 or γ_1 by the extent of the range used, the variation in δ_1 is small. As an internal consistency check of the data, there is, as expected, reasonable agreement between the values of δ_1 shown in Table 1 and those that would be estimated from the values of α_1, β_1, and γ_1 using equation (10). The tabulated values of δ_1 suggest that, at the wall, the correlation between u and $-\theta$ is perfect or nearly so.

PROBABILITY DENSITY FUNCTIONS

In view of the strong correlation between u and θ in the near-wall region, it seemed appropriate to compare, more generally, the properties of u with those of θ in this region. We consider in this section individual and joint probability density functions of these two quantities. In the following section, we briefly consider individual and cross-spectral density functions, focusing on features that have not attracted previous attention or discussion in the literature.

Individual probability density functions (pdfs) of u and $-\theta$ are shown in Fig. 3 at three positions in the near-wall region: within the sublayer ($y^+ \simeq 2.7$), at $y^+ \simeq 15$ (where $\overline{u^2}$ and the production of turbulent energy are about maximum) and near the outer edge of the buffer layer ($y^+ \simeq 40$). In view of the negative correlation between u and θ, $\hat{p}(-\theta)$ is used instead of

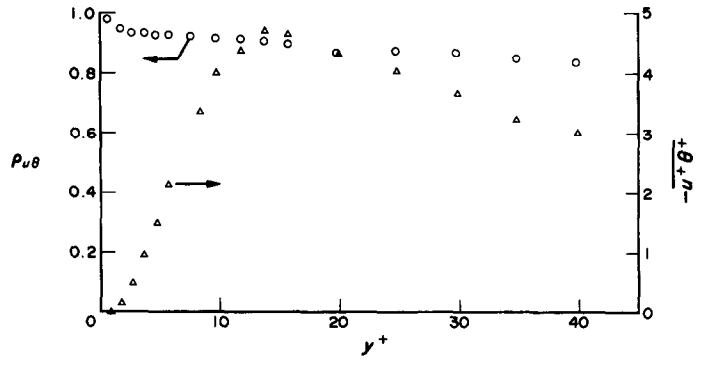

FIG. 2. Present data for the longitudinal heat flux $-\overline{u^+\theta^+}$ and the correlation coefficient $\rho_{u\theta}$ in the near-wall region: △, $-\overline{u^+\theta^+}$; ○, $\rho_{u\theta}$.

Table 1. Estimated values of coefficients α_1, β_1, γ_1, δ_1 for different y^+ ranges

	Equation	$0 < y^+ \leqslant 5$	$0 < y^+ \leqslant 6$	$0 \leqslant y^+ \leqslant 8$
α_1	6	−0.077	−0.077	−0.083
β_1	7	0.34	0.31	0.29
γ_1	8	0.26	0.26	0.26
δ_1	9	1.02	1.0	1.0

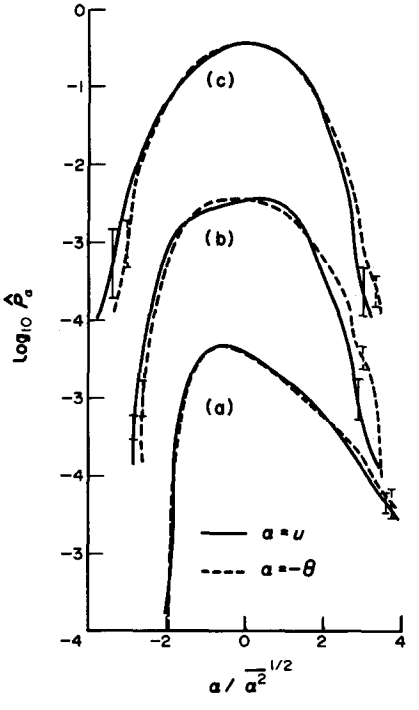

FIG. 3. Probability density functions of u and $-\theta$. (a) $y^+ \simeq 2.7$: $S(u) = 0.82$; $S(-\theta) = 0.97$; $F(u) = 3.61$; $F(-\theta) = 4.12$. (b) $y^+ \simeq 16$: $S(u) = -0.06$; $S(-\theta) = 0.21$; $F(u) = 2.36$; $F(-\theta) = 2.51$. (c) $y^+ = 40$: $S(u) = -0.22$; $S(-\theta) = -0.06$; $F(u) = 2.72$; $F(-\theta) = 2.63$. (Note the shift in origin for the ordinate.) Vertical bars represent experimental uncertainties near the tails of $\hat{p}(u)$ and $\hat{p}(-\theta)$.

$\hat{p}(\theta)$ to facilitate the comparison with $\hat{p}(u)$. A logarithmic scale is used for the ordinate to emphasize the tails of the pdfs. The main feature of Fig. 3(a) is the close similarity, for negative values of u or positive values of θ, between $\hat{p}(u)$ and $\hat{p}(-\theta)$. This similarity reflects to a large extent the similarity in the boundary conditions. At very large positive values of u, $\hat{p}(-\theta)$ is consistently larger than $\hat{p}(u)$, as is reflected by the larger magnitudes of the skewness and flatness factors of temperature than of velocity (see caption to Fig. 3). At $y^+ \simeq 15$, $\hat{p}(u)$ is very nearly symmetrical while $\hat{p}(-\theta)$ continues to be larger than $\hat{p}(u)$ for large positive values of u. The pdf of θ becomes symmetrical at larger values of y^+, in this case $y^+ \simeq 25$, an observation established in previous work (e.g. refs. [8, 16, 17]). At still larger values of y^+ (e.g. Fig. 3(c)), the skewness of θ becomes positive and of opposite sign to that of u, reflecting, as noted by ref. [18], the importance of the ejection of low momentum, high-temperature fluid from the inner part of the buffer layer. Whilst the relative behaviour, of $\hat{p}(u)$ and $\hat{p}(-\theta)$ reported by ref. [18] for the near-wall region is in qualitative agreement with the present observations, there are important quantitative differences between Zaric's data and the present data especially close to the wall. At $y^+ = 1.97$, Zaric found that the negative tail $\hat{p}(u)$ does not extend as far as that of $\hat{p}(-\theta)$ while the peak value of $\hat{p}(u)$ is 75% larger than that of $\hat{p}(-\theta)$.

More insight into the relative behaviour of u and θ within the sublayer can be inferred from the joint probability density function $\hat{p}(u,\theta)$. The plots of Fig. 4 highlight the narrowness of the iso-probability contours, especially in quadrant 2 ($u < 0$, $\theta > 0$). In the region $y^+ \gtrsim 15$, this quadrant identifies low velocity hot fluid moving towards the outer part of the buffer layer. Ejections or the sudden outward motions of low-speed streaks which have been lifted away from the wall would fall in this quadrant. Closer to the wall, it would be more appropriate to associate quadrant 2 mainly with low-speed wall streaks. At $y^+ = 2.7$, the signals u and θ are found in this quadrant for approximately 52% of the total record duration (Fig. 5). The rest of the time is accounted for as follows: 38% in quadrant 4 ($u > 0$, $\theta < 0$) and about 5% in each of the other quadrants (1 and 3). The contribution from quadrant 2 to the heat flux $-\overline{u\theta}$ is only about 38%

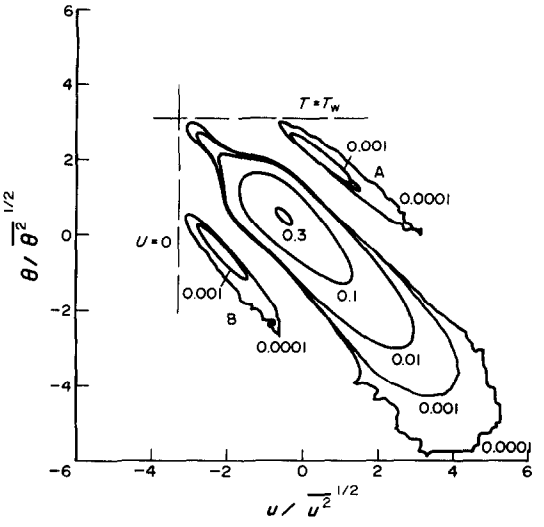

FIG. 4. Joint probability density function of u and θ at $y^+ = 2.7$.

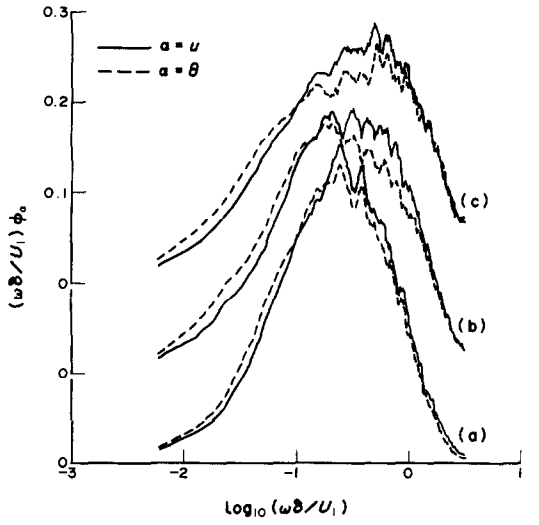

FIG. 6. Spectra of u and θ: (a) $y^+ = 2.7$; (b) $y^+ = 16$; (c) $y^+ = 40$. (Note the shift in origin for the ordinate.)

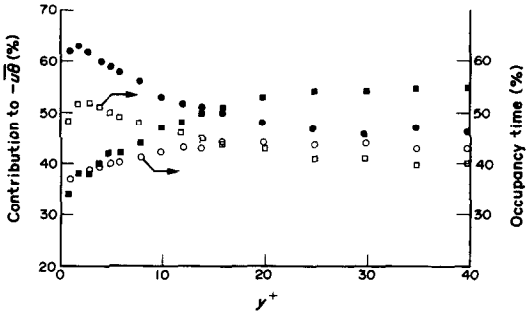

FIG. 5. Occupancy time and contribution to $-\overline{u\theta}$ from quadrants 2 and 4 in the near-wall region. Occupancy time: □, quadrant 2; ○, quadrant 4. Contribution to $-\overline{u\theta}$: ■, quadrant 2; ●, quadrant 4.

although the largest values of $\hat{p}(u,\theta)$ occur in that quadrant. The location, in quadrant 2, of the extremum in $\hat{p}(u,\theta)$ is close to the origin (i.e. $U = \bar{U}$, $T = \bar{T}$). By contrast, the contribution from quadrant 4 is large ($\simeq 62\%$) illustrated by the stretching out of the contours in that quadrant towards large values of u and θ. As shown in Fig. 5, contributions from quadrants 2 and 4 to $-\overline{u\theta}$ become equal at $y^+ \simeq 15$ while quadrant 2 dominates at larger values of y^+. This trend supports the relative contributions to $-\overline{uv}$ from quadrants 2 and 4 obtained in a fully developed duct flow [19]. Contributions from quadrants 1 and 3 are negligible throughout the near-wall region.

It is worth commenting on the existence of the contours, which are labelled A and B in Fig. 4. These contours are parallel and on either side of the main contours. They are associated with very small magnitude local peaks of $\hat{p}(u,\theta)$. Contours A and B reside only partly in quadrant 2, with contours A stretching out into quadrant 1 and contours B into quadrant 3. Contours A, B as well as the main contours are bounded at large negative values of u or positive values of θ by the physical values of the velocity and of the temperature at the wall. These latter values are indicated by the straight lines in the figure. The existence of A and B suggests a trimodal form of $\hat{p}(u,\theta)$. Note however that the locations of A and B are such that conditional pdfs $\hat{p}(u/\theta)$ or $\hat{p}(\theta/u)$, calculated for fixed values of u or θ, would be mainly bimodal. We can speculate that A and B partly reflect the intermittent nature of the near-wall flow since prolonged periods of calm, where $U \simeq 0$ and $T \simeq T_w$, should ideally show up as local peaks near the locations of the broken lines in Fig. 4. More speculatively, contours A and B may also reflect the presence of longitudinal vortices which lie on either side of a low-speed streak and are thought to be responsible for its formation.

SPECTRAL DENSITY FUNCTIONS

Spectra of u and θ were calculated for all the data in the near-wall region. Distributions for only three values of y^+ are shown in Fig. 6 since they reflect reasonably well the variation that occurs between the wall and the outer part of the buffer layer. Spectra are presented using a logarithmic abscissa for $\omega\delta/U_1$ and a linear ordinate for the product $(\omega\delta/U_1)\,\phi_\alpha$, where $\alpha \equiv u$ or θ. The area under any section of the curves in Fig. 6 is directly proportional to the fraction of total $\overline{u^2}$ or $\overline{\theta^2}$ in that particular frequency range. At $y^+ \simeq 2.7$, the distributions of $\omega\phi_u$ and $\omega\phi_\theta$ follow each other closely to within the experimental uncertainty. As y^+ increases, the spectra become less and less similar. This trend is not surprising: ref. [20] showed that for $y^+ \gtrsim 16$, a close spectral analogy exists between the velocity vector fluctuation, rather than just the longitudinal velocity fluctuation, and the temperature fluctuation. It was noted however that, as the wall

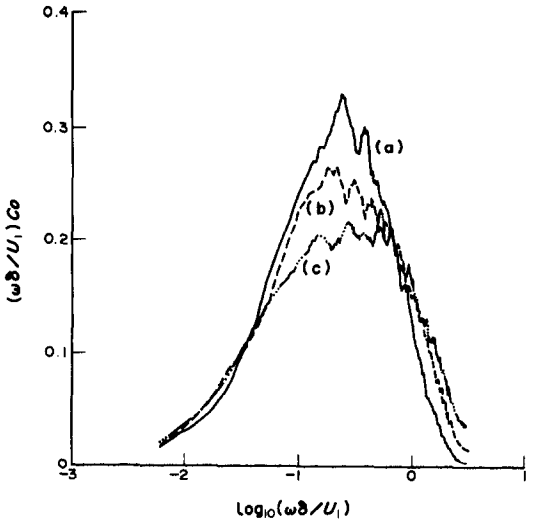

FIG. 7. Co-spectra of u and θ: (a) $y^+ = 2.7$; (b) $y^+ = 16$; (c) $y^+ = 40$.

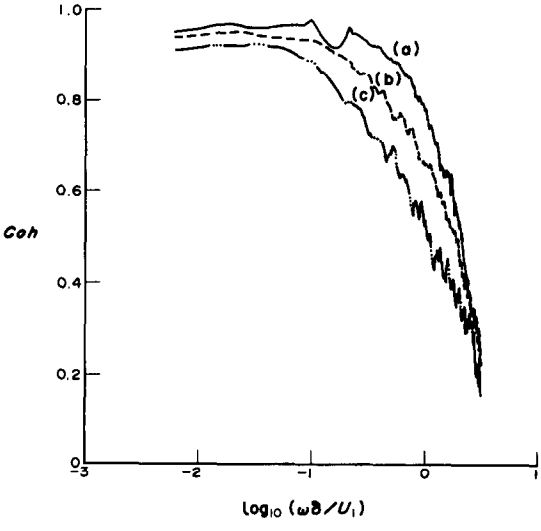

FIG. 8. Spectral coherence between u and θ: (a) $y^+ = 2.7$; (b) $y^+ = 16$; (c) $y^+ = 40$.

is approached, the difference between $\omega\phi_u$ and $\omega\phi_\theta$ practically disappeared. At $y^+ \to 0$, $\overline{u^2} \gg \overline{w^2} \gg \overline{v^2}$ so that $\overline{u^2}$ becomes a close approximation to the variance of the fluctuating velocity vector. Figure 6 indicates that a close spectral analogy can be expected between u and θ at the wall. This is supported by the physical evidence: although low-speed streaks oscillate in a spanwise direction, their ubiquitous streamwise coherence supports the relative dominance of u over w.

As y^+ increases (Fig. 6), the magnitude of the peak decreases while its position tends to shift towards higher frequencies. This trend is also discernible in the co-spectrum Co between u and θ plotted in Fig. 7 where the method of presentation is the same as in Fig. 6. The shift, in both Figs. 6 and 7 towards higher frequencies may reflect the contribution from the ejection phase of the bursting cycle. Speculatively, the larger peak at $y^+ = 2.7$ would be associated mainly with the sweep phase of the bursting cycle. Figure 8 indicates that the magnitude of the spectral coherence between u and θ is very nearly unity at $y^+ \simeq 2.7$. The frequency range over which Coh is constant increases as y^+ decreases. Bremhorst and Bullock [4] argued that their large values of the spectral correlation coefficient $Co/(\phi_u\phi_\theta)^{1/2}$ close to the wall may be due to either the longitudinal persistence of the streaks or to large-scale low wave number phenomena that extend throughout the whole flow.

CONCLUSION

The correlation coefficient between the longitudinal velocity fluctuation and the temperature fluctuation is large throughout the near-wall region. Its magnitude approaches unity at the wall in a manner consistent with the trend suggested by Taylor series expansions of u, θ and the product $u\theta$.

Individual probability and spectral density functions of u and θ reinforce the close similarity that exists between these two quantities close to the wall. Joint probability density functions of u and θ and a related quadrant analysis underline the importance of the low-speed or high-temperature streaks in terms of space occupancy but not in terms of its contribution to the longitudinal heat flux close to the wall. The largest contribution to this flux is associated with higher speed or lower temperature fluid.

Acknowledgement—The support of the Australian Research Grants Scheme is gratefully acknowledged.

REFERENCES

1. S. Corrsin, Some current problems in turbulent shear flows, Naval Hydrodynamics Publ. 515, National Academy of Sciences/National Research Council, U.S.A., pp. 373–400 (1957).
2. S. J. Kline, W. C. Reynolds, F. A. Schraub and P. W. Runstadler, The structure of turbulent boundary layers, *J. Fluid Mech.* **30**, 741–773 (1967).
3. A. F. Orlando, R. J. Moffat and W. M. Kays, Turbulent transport of heat and momentum in a boundary layer subject to deceleration, suction and variable wall temperature, Report HMT-17, Thermosciences Division, Department of Mechanical Engineering, Stanford University (1974).
4. K. Bremhorst and K. J. Bullock, Spectral measurements of temperature and longitudinal velocity fluctuations in fully developed pipe flow, *Int. J. Heat Mass Transfer* **13**, 1313–1329 (1970).
5. L. Fulachier, Contribution à l'étude des analogies des champs dynamique et thermique dans une couche limite turbulente: effet de l'aspiration, Thèse de Doctorat ès Sciences, Université de Provence (1972).
6. D. S. Johnson, Velocity and temperature fluctuation measurements in a turbulent boundary layer downstream of a stepwise discontinuity in wall temperature, *J. Appl. Mech.* 325–336 (September 1959).
7. M. Hishida and Y. Nagano, Structure of turbulent velocity and temperature fluctuations in fully developed pipe flow, *J. Heat Transfer* **101**, 15–22 (1979).
8. M. Eléna, Etude des champs dynamique et thermique d'un écoulement turbulent en conduite avec aspir-

ation à la paroi, Thèse de Doctorat ès Sciences, I.M.S.T., Université d'Aix-Marseille II (1975). Also Rapport C.E.A., R-4843 (1977).
9. Y. Iritani, N. Kasagi and M. Hirata, Heat transfer mechanism and associated turbulence structure in the near-wall region of a turbulent boundary layer. In *Turbulent Shear Flows 4* (Edited by L. J. S. Bradbury, F. Durst, B. E. Launder, F. W. Schmidt and J. H. Whitelaw), pp. 223–234. Springer, Berlin (1985).
10. L. V. Krishnamoorthy and R. A. Antonia, Temperature dissipation measurements in a turbulent boundary layer, *J. Fluid Mech.* **176,** 265–281 (1987).
11. M. Hishida and Y. Nagano, Simultaneous measurements of velocity and temperature in nonisothermal flows, *J. Heat Transfer* **100,** 340–345 (1978).
12. L. V. Krishnamoorthy and R. A. Antonia, Temperature variance and kinetic energy budgets in the near-wall region of a turbulent boundary layer, *Proc. 9th Australasian Fluid Mechanics Conference*, Auckland, New Zealand, pp. 121–124 (1986).
13. K. Hanjalic and B. E. Launder, Contribution towards a Reynolds-stress closure for low-Reynolds number turbulence, *J. Fluid Mech.* **74,** 593–610 (1976).
14. D. R. Chapman and G. D. Kuhn, The limiting behaviour of turbulence near a wall, *J. Fluid Mech.* **170,** 265–292 (1986).
15. A. A. Townsend, *The Structure of Turbulent Shear Flow*, 1st Edn. Cambridge University Press, Cambridge (1956).
16. R. A. Antonia and H. Q. Danh, Structure of temperature fluctuations in a turbulent boundary layer, *Physics Fluids* **20,** 1050–1057 (1977).
17. R. A. Antonia, A. J. Chambers and M. Eléna, Points of symmetry in turbulent shear flows, *Int. Commun. Heat Mass Transfer* **10,** 395–402 (1983).
18. Z. Zaric, Wall turbulence structure and convection heat transfer, *Int. J. Heat Mass Transfer* **18,** 831–842 (1975).
19. J. W. Wallace, H. Eckelmann and R. S. Brodkey, The wall region in turbulent shear flow, *J. Fluid Mech.* **54,** 39–48 (1972).
20. L. Fulachier and R. Dumas, Spectral analogy between temperature and velocity fluctuations in a turbulent boundary layer, *J. Fluid Mech.* **77,** 257–277 (1976).

CORRELATION ENTRE LA FLUCTUATION DE VITESSE LONGITUDINALE ET CELLE DE TEMPERATURE DANS LA REGION PARIETALE D'UNE COUCHE LIMITE TURBULENTE

Résumé—Des mesures de fluctuation de vitesse longitudinale u et de fluctuation de la température θ dans une couche limite turbulente indiquent une forte corrélation entre u et θ au voisinage immédiat de la paroi, la valeur absolue du coefficient de corrélation approchant l'unité sur la paroi. L'importance de veines à faible vitesse et forte température est examinée et quantifiée en considérant la probabilité liée et les fonctions de densité spectrale de u et θ.

KORRELATION ZWISCHEN DEN SCHWANKUNGSGRÖSSEN VON LÄNGSGESCHWINDIGKEIT UND TEMPERATUR IM WANDNAHEN GEBEIT EINER TURBULENTEN GRENZSCHICHT

Zusammenfassung—Die Messungen der Schwankungsgrößen u der Längsgeschwindigkeit und θ der Temperatur in einer turbulenten Grenzschicht weisen auf eine ausgeprägte Korrelation zwischen u und θ in der unmittelbaren Nähe der Wand hin, der absolute Wert des Korrelations-Koeffizienten an der Wand nähert sich Eins. Die Bedeutung von Strähnen kleiner Geschwindigkeit oder hoher Temperatur wurde geprüft und durch Vergleichen der Verbindungswahrscheinlichkeit und der spektralen Dichte-Funktion von u und θ quantifiziert.

КОРРЕЛЯЦИЯ МЕЖДУ ФЛУКТУАЦИЯМИ ПРОДОЛЬНОЙ КОМПОНЕНТЫ СКОРОСТИ И ТЕМПЕРАТУРЫ В ПРИСТЕННОЙ ОБЛАСТИ ТУРБУЛЕНТНОГО ПОГРАНИЧНОГО СЛОЯ

Аннотация—Измерениями флуктуаций продольной компоненты скорости u и температуры θ в туробулентном пограничном слое установлена тесная корреляция между величинами u и θ в непосредственной близости от стенки, причем абсолютное значение коэффициента корреляции приближается на стенке к единице. Проанализирована роль примесей малой скорости или высокой температуры и дана их численная оценка путем совместного рассмотрения функций вероятности и спектральной плотности указанных величин.